

A simple energy loss model and its applications for silicon detectors

Ferenc Siklér

*KFKI Research Institute for Particle and Nuclear Physics, Budapest, Hungary
CERN, Geneva, Switzerland*

Abstract

The energy loss of charged particles in silicon can be approximated by a simple analytical model. With help of measured charge deposits in individual channels of hit clusters their position and energy can be estimated. Deposits below threshold and saturated values are treated properly, resulting in a wider dynamic range. The proposed method gives improvements on both hit position and energy residuals. The model is successfully applied to track differential energy loss estimation and to detector gain calibration tasks.

Keywords: Energy loss, Silicon

PACS: 29.40.Gx, 29.85.-c, 34.50.Bw

1. Introduction

The identification of charged particles is essential in several fields of particle and nuclear physics: particle spectra, correlations, selection of daughters of resonance decays and for reducing the background of rare physics processes [1, 2]. Silicon detectors can be employed for identification by proper use of energy deposit measurements along the trajectory of the particle. The aim of this study is to provide a simple method to evaluate energy deposits and other derived quantities for a wide range of particle momenta ($\beta\gamma = p/m = 0.56 - 10.0$) and detector thickness, based on the precise knowledge of the known underlying physics processes.

This article is organized as follows: the model is motivated and discussed in detail in Sec. 2. Among the various applications we will deal with the estimation of hit position (Sec. 3), hit energy deposit (Sec. 4), differential energy loss for tracks (Sec. 5), as well as detector gain calibration for tracks (Sec. 6). This work ends with conclusions.

2. Simple energy loss model

When a charged particle traverses material it loses energy in several discrete steps, dominantly by resonance excitations (δ -function) and Coulomb excitations (truncated $1/E^2$ term). This latter is the reason for the long tail observed in energy deposit distributions. It is generally difficult to describe the process with a simple function. The most probable energy loss Δ , and the full width of the energy loss distribution at half maximum Γ_Δ [3] can be approximated by

$$\Delta = \xi \left[\log \frac{2mc^2\beta^2\gamma^2\xi}{I^2} + 0.2000 - \beta^2 - \delta \right] \quad (1)$$

$$\Gamma_\Delta = 4.018\xi$$

where

$$\xi = \frac{K}{2} z^2 \frac{Z}{A} \rho \frac{l}{\beta^2}$$

Email address: sikler@rmki.kfki.hu (Ferenc Siklér)

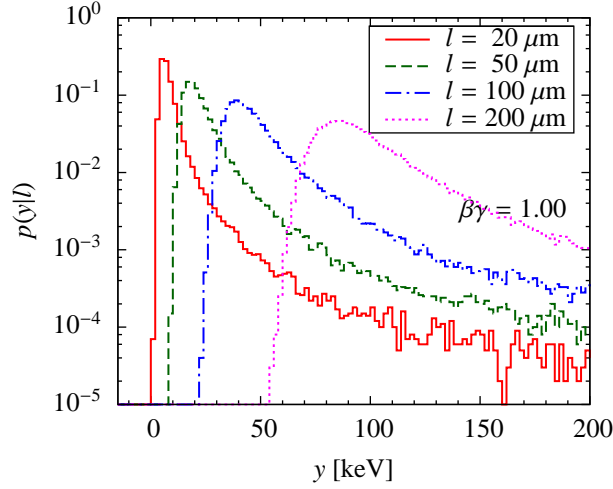


Figure 1: Probability density functions for particles with $\beta\gamma = 1.00$, at given path lengths of 20, 50, 100 and 200 μm .

is the Landau parameter; $K = 4\pi N_A r_e^2 m_e c^2 = 0.307\,075\text{ MeV cm}^2/\text{mol}$; Z , A , ρ and l are the mass number, atomic number, density and thickness of the material, respectively; and δ is the density correction [4].

The probability of an excitation, energy deposit, along the path of the incoming particle is a function of $\beta\gamma = p/m$ of the particle and depends on properties of the traversed material. The conditional probability density $p(y|l)$, deposit y along a given path length l , can be built using the above mentioned elementary excitations combined with an exponential occurrence model. The details of the microscopical simulation for silicon can be found in Refs. [3], [5] and [6]. The result of these recursive convolutions is a smooth function (Fig. 1).

In the experiment the deposit values y are measured. For a fixed y the conditional probability can be regarded as function of l , thus $p(y|l) \equiv f_y(l)$. Values of $f_y(l)$ for particles with $\beta\gamma = 3.16$ are plotted in Fig. 2, where the values corresponding to $y = 50, 100, 200$ and 300 keV are shown. Other $\beta\gamma$ settings show very similar behavior ($\beta\gamma = 0.56, 1.00$ and 10.0 , not plotted). Apart from a multiplicative factor, they are well approximated by a combination of simple functions, exponential and Gaussian:

$$f_y(l) \propto \begin{cases} \exp\left(\frac{\nu(l-l_P)}{\sigma_l} + \frac{\nu^2}{2}\right), & \text{if } l < l^* \\ \exp\left(-\frac{(l-l_P)^2}{2\sigma_l^2}\right), & \text{if } l \geq l^* \end{cases} \quad (2)$$

where the limit is

$$l^* = l_P - \nu\sigma_l.$$

The peak position l_P and standard deviation σ_l are both functions of y and $\beta\gamma$, $\nu \approx 0.65$ is constant. Note that f_y is constructed such that the value and the derivative are continuous at the limit l^* . The peak position l_P is roughly proportional to the deposit y , their relationship can be approximated as

$$y \approx \varepsilon l_P [1 + 0.08 \log(l_P/l_0)] \quad (3)$$

where l_0 is some *reference path length* (Fig. 3). In this work $l_0 = 300\text{ }\mu\text{m}$ was chosen. At the same time σ_l has an approximate first order polynomial dependence on y (Fig. 4).

As it was shown above, some interesting connections between the deposit and path length can be observed, for wide range of $\beta\gamma$ values. Unfortunately the dependence on $\beta\gamma$, and l , is still present. In the following (Sec. 2.1) we will show how that can be suppressed or even eliminated.

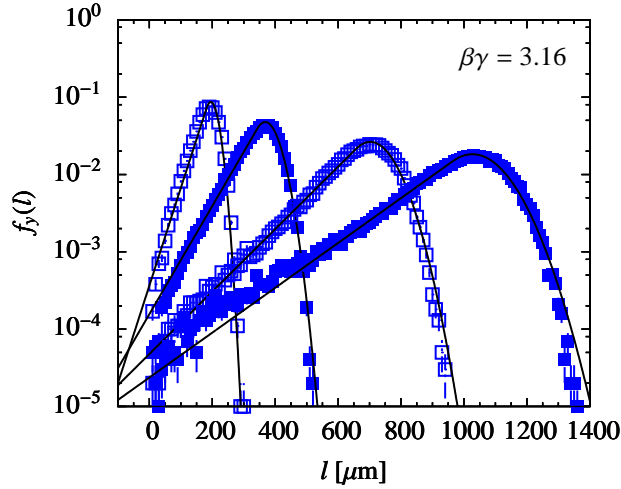


Figure 2: Fits of the conditional probability density $f_y(l)$ as function of the path length l for particles with $\beta\gamma = 3.16$ (see Eq.(2)). The simulated values (points) and the fitted curves (lines) corresponding to $y = 50, 100, 200$ and 300 keV are shown, from left to right.

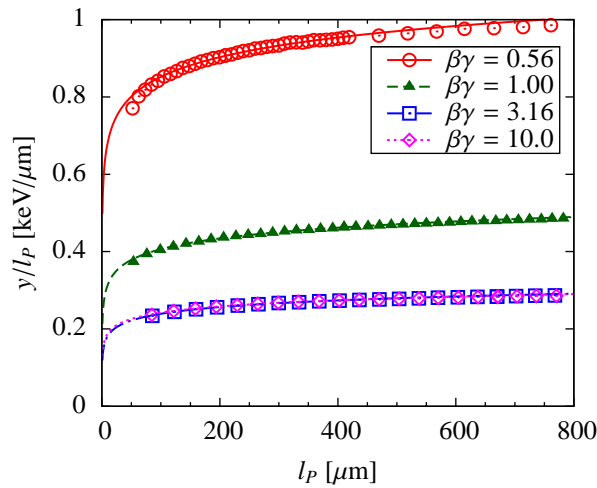


Figure 3: Relationship between the measured deposited energy y and the position of the path length peak l_p , shown together with fits using Eq. 3.

2.1. Most probable differential energy loss

The path length dependence of the most probable energy loss Δ (Fig. 5) has a form that is very similar to Eq. (3). The dependence can be approximated by

$$\Delta(l) \approx \varepsilon l [1 + a \log(l/l_0)] \quad (4)$$

where ε is the *most probable differential energy loss* along a reference length l_0 , hence $\varepsilon = \Delta(l_0)/l_0$. For the relevant $\beta\gamma$ region studied in this paper $a \approx 0.07$, to a good approximation.¹ For some applications, such as hit position estimation, the assumption of linearity may be enough (see Eq. (17) later).

Hence it is worthwhile to check whether the dependence on $\beta\gamma$ and l can be suppressed by taking the most probable deposit Δ as variable of the conditional probability. Values of $p(y|\Delta) \equiv f_y(\Delta)$ for particles with $\beta\gamma = 0.56, 1.00, 3.16$

¹Based on Eq. 1, with some approximations, the expected magnitude of a would be $1/\log(2m_e c^2 K z^2 \cdot Z/A \cdot \rho/l^2) \approx 0.064$.

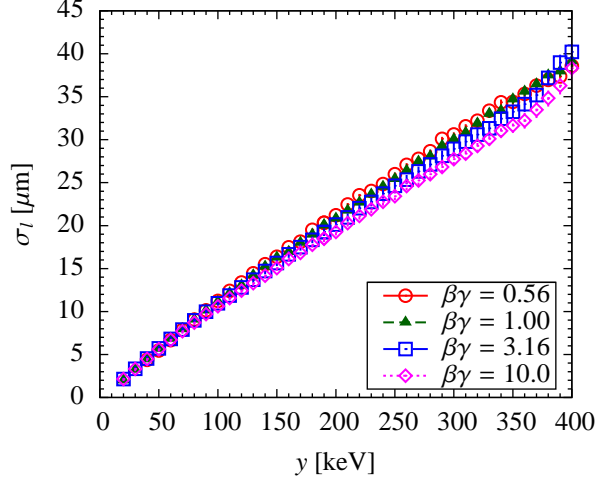


Figure 4: Relationship between the measured deposited energy y and the standard deviation σ_l of l distribution.

and 10.0 are plotted in Fig. 6, where the values corresponding to $y = 50, 100, 200,$ and 300 keV are shown. The distributions for a given y value are remarkably similar for all $\beta\gamma$ values.

The conditional probability density for a given y , as a function of Δ can be described as

$$f_y(\Delta) \approx C(y) \cdot \begin{cases} \exp\left(\frac{\nu(\Delta-y)}{\sigma_\Delta} + \frac{\nu^2}{2}\right), & \text{if } \Delta < \Delta^* \\ \exp\left(-\frac{(\Delta-y)^2}{2\sigma_\Delta^2}\right), & \text{if } \Delta \geq \Delta^* \end{cases} \quad (5)$$

where $C(y)$ is a universal function of y . Note that f_y is constructed such that the value and the derivative are continuous at the limit Δ^* that is given by

$$\Delta^*(y) = y - \nu\sigma_\Delta(y) \quad (6)$$

where $\nu \approx 0.65$ is constant. Fig. 7-left shows that σ_Δ is a first order polynomial of y , practically independent of $\beta\gamma$, in the form

$$\sigma_\Delta(y) = \sigma_0 + by \quad (7)$$

where $\sigma_0 \approx 2$ keV, $b \approx 0.095$. According to Fig. 7-right the y dependent coefficient of Eq. (5) is very well approximated as

$$C(y) \propto 1/\sigma_\Delta(y). \quad (8)$$

The parameters of the above detailed energy loss model and their short explanations are listed in Table 1. Note that these four numbers are the only parameters of the description. Usually the detector and readout noise can be neglected. If this is not the case the term σ_Δ^2 in Eq. (5) and (8) should be replaced by $\sigma_D^2 + \sigma_n^2$ where σ_n is the standard deviation of the Gaussian noise.

Table 1: Parameters of the energy loss model.

| | | |
|------------|-------|--|
| ν | 0.65 | Gaussian vs exponential [$\sigma_\Delta(y)$] |
| a | 0.07 | coefficient of log term in $\Delta(l)$ |
| σ_0 | 2 keV | constant term of $\sigma_\Delta(y)$ |
| b | 0.095 | linear coefficient of $\sigma_\Delta(y)$ |

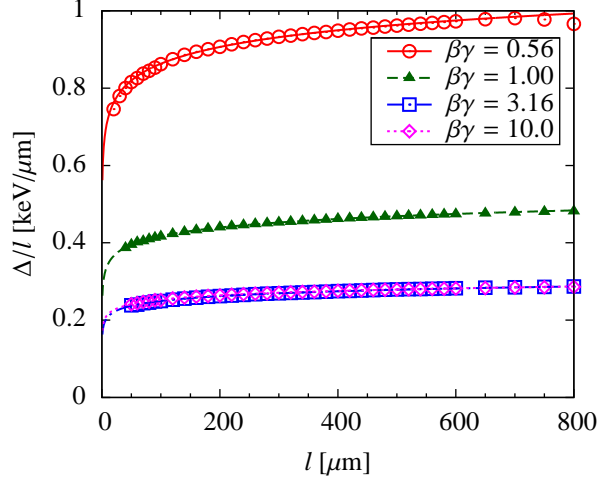


Figure 5: Relationship between the most probable energy deposit Δ and the path length l , shown together with fits using Eq. 4.

2.2. Left truncation and right censoring

During readout the deposited energy is converted to measured ADC values through several steps: primary and secondary electron-hole pairs, current signals, front-end electronics, digitization [7]. In this study we assume that the response of the detector system is linear in the threshold-to-censoring region. Signals below threshold are truncated, since they produce no output. Signals above a certain level are censored, hence only the fact that the deposit was above that level is known. Note that the censoring level does not necessarily coincides with the saturation level of the readout electronics: the former is simply chosen as the limit of linearity.

If the measured value y is below or above a limit t , the corresponding values can be calculated by integration

$$f_{y<t}(\Delta) = \int_{-\infty}^t f_y(\Delta) dy, \quad f_{y>t}(\Delta) = \int_t^{\infty} f_y(\Delta) dy.$$

Note that since σ_Δ is a function of y , the integrals are difficult to perform. The simulated values with several truncation thresholds and censoring levels are shown in Fig. 8. They are well approximated by the following functional forms:

$$f_{y<t}(\Delta) = \begin{cases} 1, & \text{if } \Delta < t - \sigma_\Delta \\ \exp\left[-\frac{1}{2}\left(\frac{\Delta-t}{\sigma_\Delta} + 1\right)^2\right], & \text{if } \Delta \geq t - \sigma_\Delta \end{cases} \quad (9)$$

$$f_{y>t}(\Delta) = \begin{cases} \exp\left[\frac{1}{2}\left(\frac{\Delta-t}{\sigma_\Delta} - 1\right)\right], & \text{if } \Delta < t + \sigma_\Delta \\ 1, & \text{if } \Delta \geq t + \sigma_\Delta. \end{cases} \quad (10)$$

2.3. Log-likelihood minimization

In summary, for a given measured deposit y the probability density will be a function of Δ only. The measure of goodness can be obtained with help of the log-likelihood value as

$$\chi^2 = -2 \log f.$$

For a given channel, with measured (y) or limited deposit values (t), the corresponding χ^2 can be derived from Eqs. (5)-

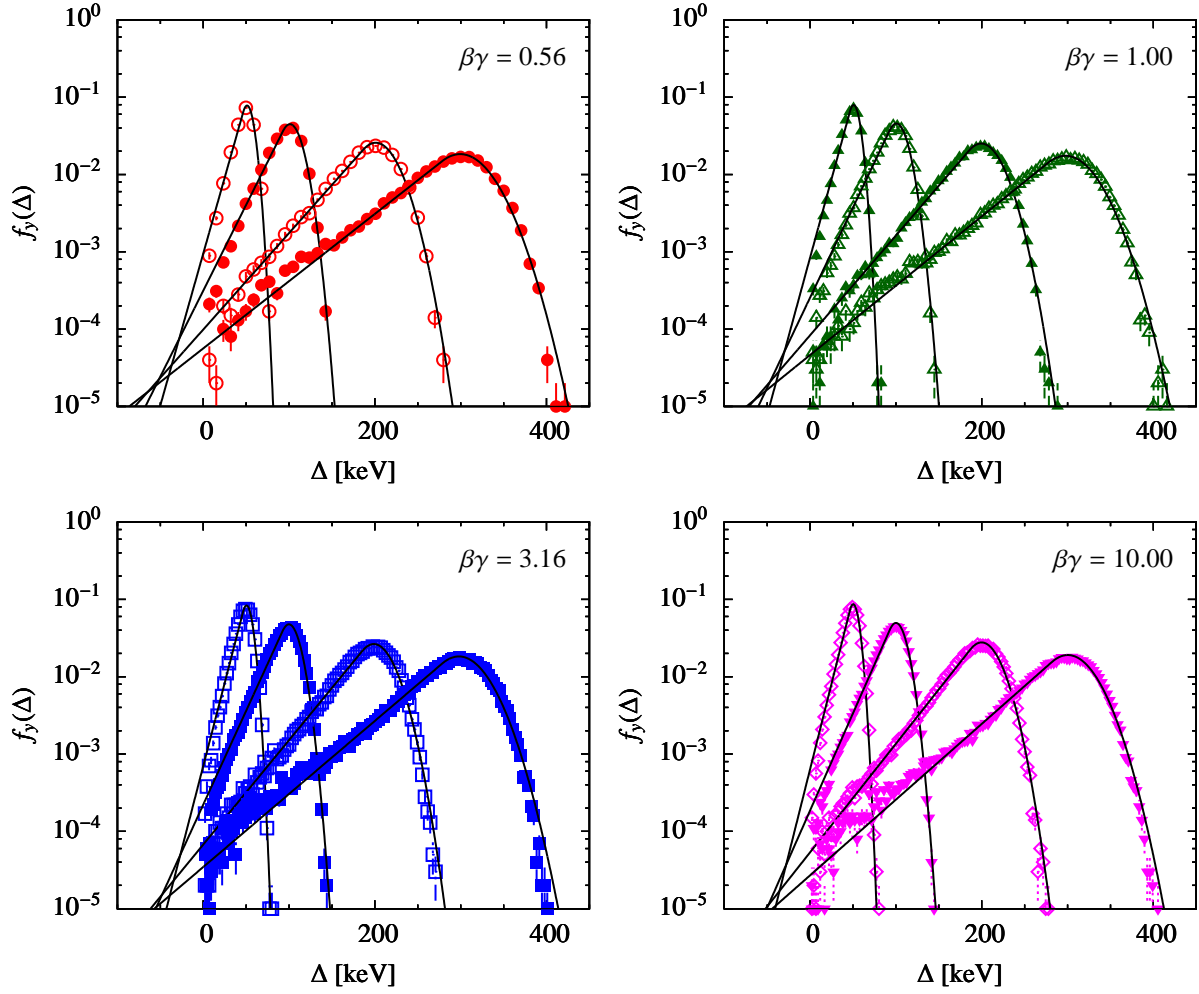


Figure 6: Fits of the conditional probability density $f_y(\Delta)$ as function of the most probable energy loss Δ for particles with $\beta\gamma = 0.56, 1.00, 3.16,$ and 10.0 (see Eq. (5)). The simulated values (points) and the fitted curves (lines) corresponding to $y = 50, 100, 200$ and 300 keV are shown, from left to right.

(8) and (9)-(10) and they are shown below:

$$\chi_y^2(\Delta) = 2 \log \sigma_\Delta(y) + \begin{cases} \frac{-2v(\Delta-y)}{\sigma_\Delta(y)} - v^2, & \text{if } \Delta < y - v\sigma_\Delta(y) \\ \left(\frac{\Delta-y}{\sigma_\Delta(y)}\right)^2, & \text{if } \Delta \geq y - v\sigma_\Delta(y) \end{cases} \quad (11)$$

$$\chi_{y < t}^2(\Delta) = \begin{cases} 0, & \text{if } \Delta < t - \sigma_\Delta(t) \\ \left(\frac{\Delta-t}{\sigma_\Delta(t)} + 1\right)^2, & \text{if } \Delta \geq t - \sigma_\Delta(t) \end{cases} \quad (12)$$

$$\chi_{y > t}^2(\Delta) = \begin{cases} -\frac{\Delta-t}{\sigma_\Delta(t)} + 1, & \text{if } \Delta < t + \sigma_\Delta(t) \\ 0, & \text{if } \Delta \geq t + \sigma_\Delta(t) \end{cases} \quad (13)$$

where $\sigma_\Delta(y)$ is given by Eq. (7). The terms on the right side contain only linear or positive definite quadratic functions of Δ . We can estimate ε for single hits or for the whole particle trajectory by minimizing the sum of corresponding chi-square values.

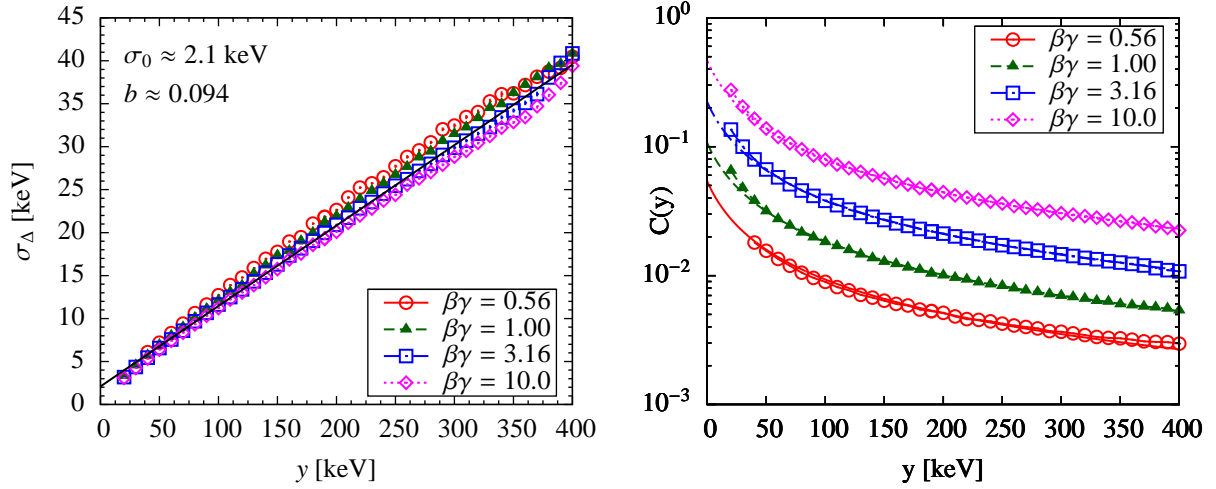


Figure 7: Left: Relationship between the measured deposited energy y and the standard deviation σ_Δ of Δ distribution. Right: The measured value of $C(y)$ for particles with $\beta\gamma = 0.56, 1.00, 3.16,$ and 10.0 . The points and curves are successively multiplied by factors of 2 for clarity. Note that the plotted function $1/\sigma_\Delta(y)$ is the same in all cases except for the multiplicative factor mentioned before.

The proposed model has several applications, such as

- for a given hit the estimation of position \mathbf{P} and energy deposit via optimizing ε and the individual path lengths l_i in the various sensitive units, channels, of the detector (Sec. 3 and 4).
- for a given trajectory the estimation of most probable differential energy loss via optimizing ε (Sec. 5).
- detector gain (cross-)calibration with tracks via the variation of the chip by chip gain, hence by modifying the y values (Sec. 6).

2.4. Estimation of parameter errors

In case of normal approximations, the inverse of the observed, sample based, Fisher information \mathcal{I} can be used to estimate the covariance of the fitted parameters V [8]:

$$\mathcal{I}_{jk} = \frac{1}{2} \frac{\partial^2 \sum_i \chi_i^2}{\partial a_j \partial a_k}, \quad V \approx -\mathcal{I}^{-1}$$

where $\sum_i \chi_i^2$ denotes the joint chi-square of hit channels or trajectory hits.

2.5. Generation of random deposits

If the expected shape of the distribution of the estimator has to be determined using Monte Carlo simulation, the generation of deposits should be fast but precise. The energy deposit distribution function

$$P(y|\Delta) \propto \frac{1}{\sigma_\Delta(y)} \cdot \begin{cases} \exp\left[-\frac{(\Delta-y)^2}{2\sigma_\Delta(y)^2}\right], & \text{if } y < \Delta + \nu\sigma_\Delta(y) \\ \exp\left[\frac{\nu(\Delta-y)}{\sigma_\Delta(y)} + \frac{\nu^2}{2}\right], & \text{if } y \geq \Delta + \nu\sigma_\Delta(y) \end{cases}$$

does not have a closed antiderivative, hence a simple inverse transform sampling is not possible. Due to its long high energy tail the acceptance-rejection method is also highly ineffective.

Let us suppose that we have generated a random deposit y_0 at a given Δ_0 . The value y_0 can be simply transformed to get a proper random deposit y for Δ with a linear transformation as

$$\frac{y - \Delta}{\sigma_\Delta(\Delta)} = \frac{y_0 - \Delta_0}{\sigma_\Delta(\Delta_0)}$$

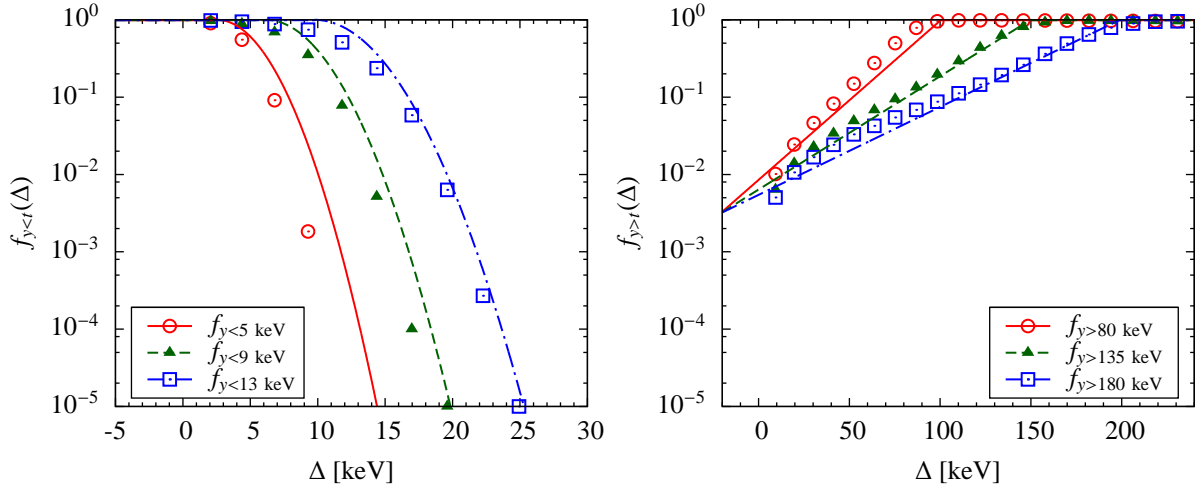


Figure 8: Fits of the conditional probability $f_{y \leq t}(\Delta)$ for measurements below threshold (left) and above censoring level (right) as function of Δ , in case of several limiting values. Examples thresholds are 5, 9 and 13 keV, while censoring levels are at 80, 135 and 180 keV. The simulated values (points) are shown for particles with $\beta\gamma = 3.16$, together with the fitted curves (lines, from Eqs. (9) and (10)).

The distribution of y can be deduced from $P(y_0|\Delta_0)$ and it can be shown that it equals with $P(y|\Delta)$. The key of the proof is the identity

$$\frac{\sigma_{\Delta}(\Delta_0)}{\sigma_{\Delta}(\Delta)} \frac{\sigma_{\Delta}(y)}{\sigma_{\Delta}(y_0)} = 1.$$

3. Estimation of hit position

During the passage of a charged particle through sensitive silicon volumes one or more channels (pixels or strips) are hit. The charges created in the adjacent channels are recorded (electrons or holes), they provide input for hit cluster recognition. Here the task is to estimate the position \mathbf{P} of the hit, location of the trajectory in the central plane, using the measured deposits.

Throughout this paper it is required that the local direction of the trajectory, hence the vector of the projected passage λ (projected onto the surface layer by drift), is known (Fig. 9). In other words only the re-estimation of cluster parameters is attempted.

3.1. Standard estimation

The simplest way of hit position estimation (labeled as Weighted) is the weighted mean of channel positions \mathbf{p}_i , where weights are the corresponding energy deposits y_i :

$$\mathbf{P}_{\text{Weighted}} = \frac{\sum_i y_i \mathbf{p}_i}{\sum_i y_i}.$$

Another widely used standard reconstruction technique (labeled as First-last) deals only with one dimensional clusters [9, 10]. This treatment is natural for strip detectors. For pixels the cluster is projected onto both directions (x and y) and the two projections are analyzed separately. Only the first and last, projected and summed, channels are used for position determination, because that choice reduces the sensitivity to fluctuations in energy deposition. If the energy would be lost steadily, the estimated projected hit position would be

$$\mathbf{P}_{\text{First-last}} = \frac{\mathbf{p}_F + \mathbf{p}_L}{2} + \frac{y_L - y_F}{2(y_L + y_F)} \lambda_{eff}$$

where the x and y components of λ_{eff} are the sum of the path lengths in the two corresponding edge channels. The above formula can be further corrected for the drift direction if the silicon was placed in magnetic field.

Due to the use of projections, relevant informations corresponding to the shape of hit cluster and its deposits are lost. In this work a new method is presented which takes each individual channel of the cluster into account.

3.2. Estimation using the model

The passage of a charged particle through the silicon layer is given by the entry and exit points of its trajectory. Even in magnetic field or for very slow particles the passage is very well approximated by a straight line, the entry and exit points being on different sides of the layer. The deposited charge along the passage is projected onto the surface layer by drift, as result of electric and magnetic fields. The local direction of the particle at a silicon unit can be calculated using the parameters of the trajectory and the vector of the projected passage λ is known.

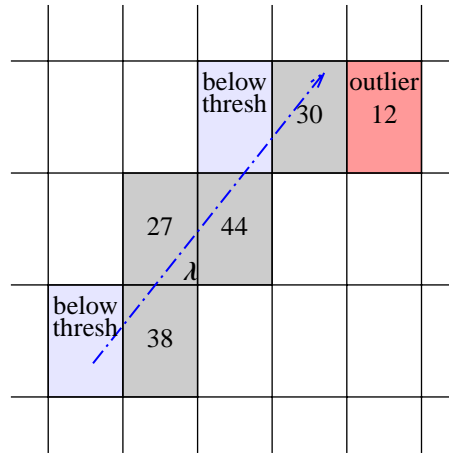


Figure 9: Example cluster with measured deposits (rounded numbers in keV) and the the projected passage λ (arrow) at some stage of the minimization. The pixels below threshold are indicated with a lighter fill (below thresh.), while the outlier pixel has a darker fill than the others.

The following discussion deals with pixel silicon detectors, but it can be easily applied to strips by taking one of the pixel dimensions to very large values. During clustering neighboring pixels (those with common edge or vertex) are grouped to form a cluster, a reconstructed hit (Fig. 9). For the analysis of the corresponding cluster two types of pixels are of importance:

- A *touched pixel* is touched by the projected passage, regardless of its measured deposit. It can belong to the cluster (non-zero deposit) but it may be an empty pixel as well, if the deposited charge was below the threshold. The intersections of the projected passage and the edges of a pixel naturally give the projected path length inside that pixel.
- An *outlier pixel* is not crossed by the projected passage but it is a member of the cluster (non-zero deposit). In other words this pixel is an outlier, mostly left by a secondary particle, often δ -electrons, created during the passage of the charged particle in the silicon. The projected passage does not have any section inside the pixel, but it is possible to construct a measure of the pixel-passage distance, a sort of negative path length (see Sec. 3.3). That notion is important in order to properly take into account the effect of charge diffusion² and to be able to move the projected path towards the outlier. This extension also ensures a smooth convergence of the minimization.

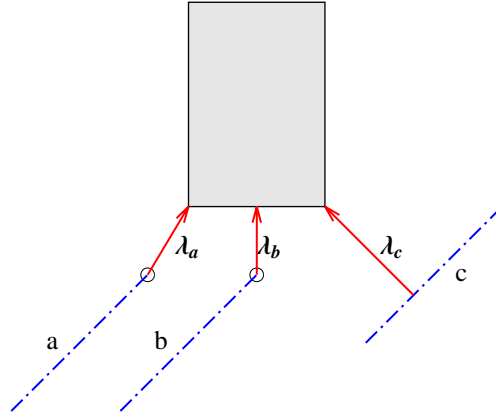


Figure 10: The three possible relative placements of projected paths (line segments) and an outlier pixel (filled rectangle). The distance of the line segment and the rectangle is shown by the corresponding arrows ($\lambda_{a,b,c}$).

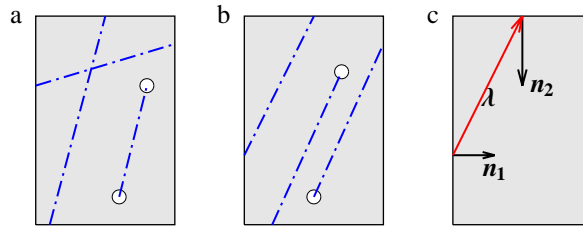


Figure 11: Line segments (dash dotted lines) on the surface of a pixel (filled rectangle). They can be bound by endpoints (open circles) or crossing points. a: The length is insensitive to small change of the hit position. b: The length changes when the hit is moved. c: Normal vectors n_1 , n_2 and the vector of the projected passage λ .

3.3. Projected path length

The task is to determine the projected path lengths λ_i for each pixel i , for a given hit position \mathbf{P} . Using the coordinates of the two endpoints, find points where the track crosses the horizontal (along x direction) or vertical (along y direction) pixel division lines. Determine the dominant direction of the cluster by choosing longer projection of the passage to the axes. Sort the endpoints and crossing points along their coordinate in the dominant direction. The lengths of the resulting line segments will give the projected path lengths λ_i for touched pixels. In case of outlier pixels determine the distance of the projected line segment to the pixel (Fig. 10) by evaluating the combinations

- two endpoints of the projected path line segment with respect to the four vertices and four edges of the pixel (cases a and b),
- projected path line segment with respect to the four vertices of the pixel (case c),

and choose the *negative* of the smallest distance. The outlined procedure ensures that by varying the hit position \mathbf{P} , the projected path lengths of touched and outlier pixels will change continuously, without jumps.

²In case of 300 μm thickness its contribution is about 5 μm .

3.4. Derivatives

How does the projected path length λ change if the hit position \mathbf{P} is varied? The corresponding line segment can be bound by endpoints or crossing points. The length is insensitive to small changes of the hit position if both points are endpoints or if both points are crossing points on opposite sides of the pixel (Fig. 11 a). The length will change only if one of the points is an endpoint or if both points are crossing points on neighboring sides of the pixel (Fig. 11 b). The derivative $\partial\lambda/\partial\mathbf{P}$ can be computed with help of the inward directed normal vectors \mathbf{n}_j at crossing points and the vector of the projected passage λ (Fig. 11 c):

$$\frac{\partial\lambda}{\partial\mathbf{P}} = \sum_j \frac{\mathbf{n}_j\lambda}{|\mathbf{n}_j\lambda|} \quad (14)$$

where the index j runs for all (0, 1 or 2) crossing points belonging to the line segment. For outliers the derivative is the unit vector

$$\frac{\partial\lambda}{\partial\mathbf{P}} = \frac{\lambda}{\lambda}. \quad (15)$$

3.5. Minimization

The joint chi-square for all channels in a hit cluster can be written as

$$\chi^2(\boldsymbol{\varepsilon}, \mathbf{P}) = \sum_i \chi_{y_i}^2(\Delta(\boldsymbol{\varepsilon}, l_i(\mathbf{P}))) \quad (16)$$

where the index i runs for all the touched and untouched channels of the hit. Note that while the deposits y_i are given, the Δ s depend on $\boldsymbol{\varepsilon}$ and the path lengths l_i inside the channels (Eq. (4)) which in turn depend on the actual hit position \mathbf{P} . The best hit position, and the most probable differential energy loss will be estimated by minimizing χ^2 . The (three dimensional) path lengths l_i can be obtained from the projected lengths λ_i as

$$l_i = \frac{l}{\lambda} \lambda_i$$

where l is the total path length and λ is the total projected length, both are fixed from the local trajectory direction.

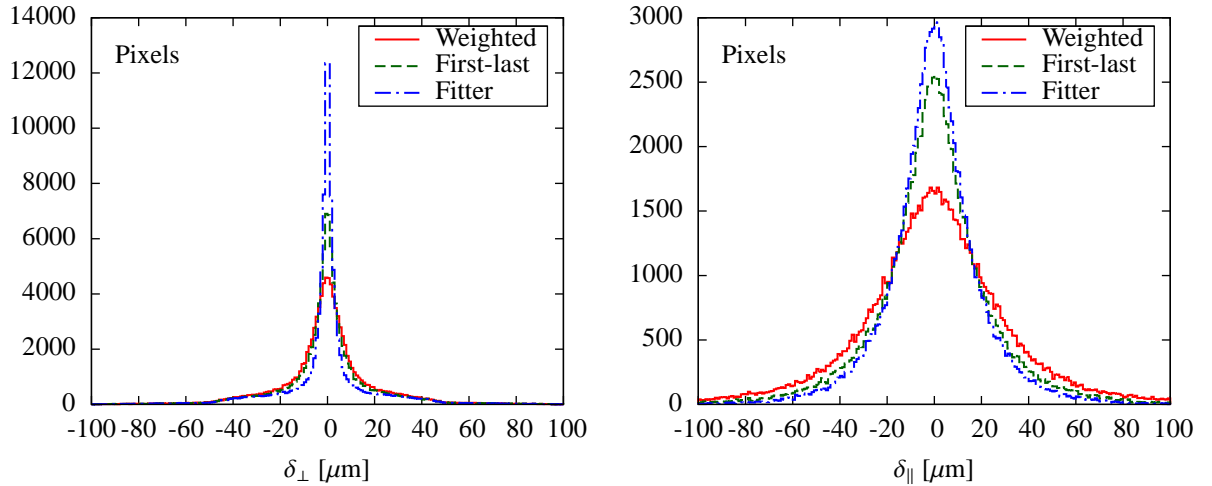


Figure 12: Residuals of the reconstructed hit position in directions perpendicular to (left) or parallel with (right) the projected trajectory using the discussed methods.

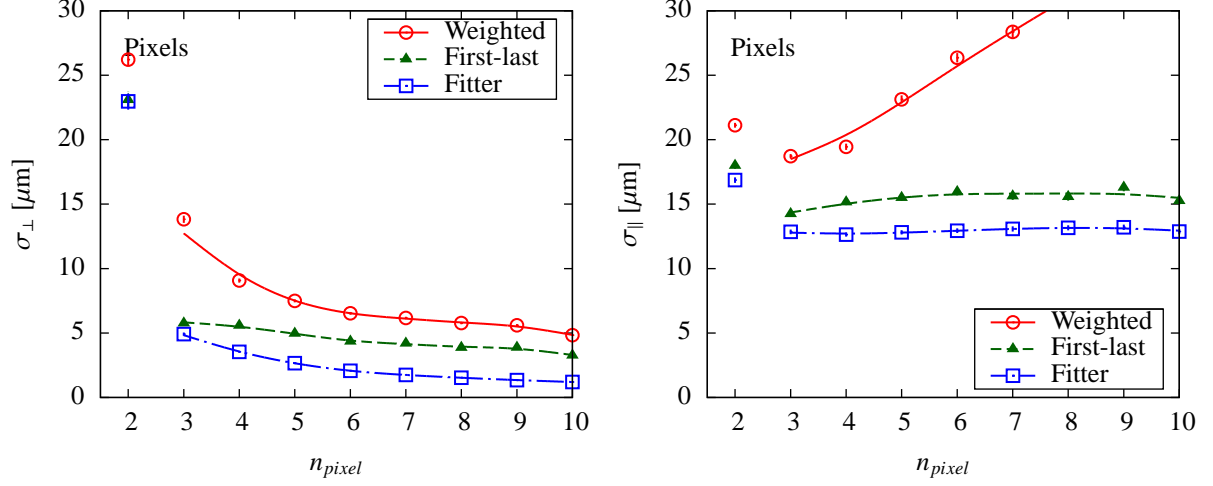


Figure 13: Resolution of the reconstructed hit position in directions perpendicular to (left) or parallel with (right) the projected trajectory using the discussed methods, as a function of the number of pixels in the cluster. Lines are drawn to guide the eye.

In case of hit position estimation the value of ε is not relevant, hence instead of the complete relationship shown in Eq. (4) a simple linearity can be assumed

$$\Delta(l) \approx \varepsilon l \quad (17)$$

where ε is rather the average rate of energy loss. The first derivatives of the χ^2 components with respect to $(\varepsilon, \mathbf{P})$ are

$$\frac{\partial \chi^2}{\partial \varepsilon} = \frac{\partial \chi^2}{\partial \Delta} l, \quad \frac{\partial \chi^2}{\partial P_j} = \frac{\partial \chi^2}{\partial \Delta} \varepsilon \frac{\partial l}{\partial P_j}$$

while the second derivatives are

$$\frac{\partial^2 \chi^2}{\partial \varepsilon^2} = \frac{\partial^2 \chi^2}{\partial \Delta^2} l^2, \quad \frac{\partial^2 \chi^2}{\partial P_j \partial P_k} = \frac{\partial^2 \chi^2}{\partial \Delta^2} \varepsilon^2 \frac{\partial l}{\partial P_j} \frac{\partial l}{\partial P_k}$$

where the term containing $\frac{\partial^2 l}{\partial \mathbf{P}^2} = 0$ is not shown. The second derivative cross-term is

$$\frac{\partial^2 \chi^2}{\partial \varepsilon \partial P_j} = \left(\frac{\partial^2 \chi^2}{\partial \Delta^2} \Delta + \frac{\partial \chi^2}{\partial \Delta} \right) \frac{\partial l}{\partial P_j}$$

The partial derivative of the path length is

$$\frac{\partial l}{\partial \mathbf{P}} = \frac{l}{\lambda} \frac{\partial \lambda}{\partial \mathbf{P}}$$

and the last term is given in Eqs. (14) and (15). During minimization the positivity of ε can be assured by choosing $\log \varepsilon$ as the free parameter. Since both the first and second derivatives can be calculated, Newton's method [11] can be used for fast and precise minimization.

In case of strips the observed signals are correlated. Before starting with the position estimation the coupling has to be undone first: it will be discussed in Sec. 4.1.

3.6. Results

For the studies in Sec. 3 and 4 charged particles in the $\beta\gamma$ range of 0.56 – 10.0 were generated with flat distribution in $\log(\beta\gamma)$, and in pseudo-rapidity, $-2.5 < \eta < 2.5$, following a $p_T \exp(-p_T/T)$ shape for the transverse momentum distribution, where $T = 0.15$ GeV/c was set. Some relevant quantities used in the simulation are given in Table 2.

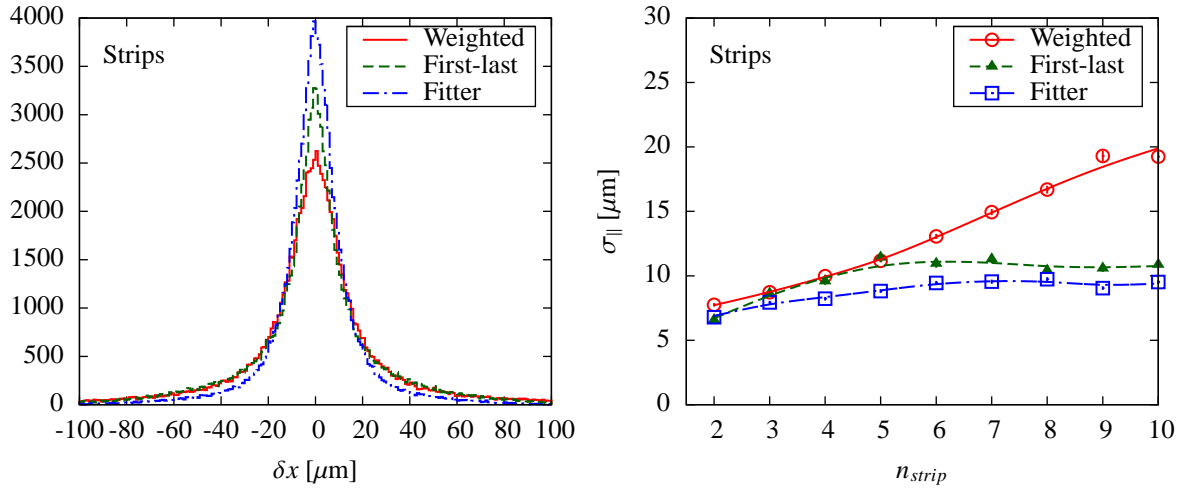


Figure 14: Residuals of the reconstructed hit position (left) and the resolution of the reconstructed hit position using the discussed methods, as a function of the number of strips in the cluster (right). Lines are drawn to guide the eye.

Table 2: Some relevant quantities used in silicon detector simulation.

| | |
|--------------------------------|-------------------|
| Detector thickness | 300 μm |
| Pitch, pixels (x direction) | 100 μm |
| Pitch, pixels (y direction) | 200 μm |
| Pitch, strips | 100 μm |
| Signal coupling, strips | 0.1 |
| Channel noise | 1.5 keV |
| Channel threshold | 7.5 keV |
| Channel saturation | 150 keV |

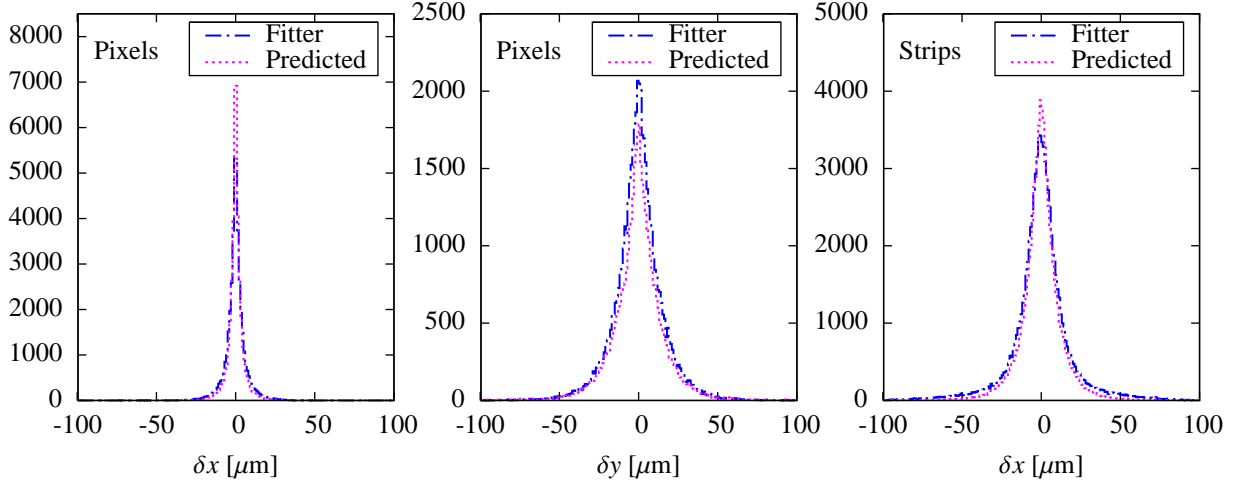


Figure 15: Residuals of the reconstructed hit position for pixels (x and y directions) and strips, from left to right. The measured values from comparison of reconstructed and simulated positions (Fitter, dash-dotted line) are shown together with the distribution predicted from the errors of the fitted parameters (Predicted, dashed line).

The pixel and strip layers were located in a barrel geometry at 10 cm and 50 cm radial distances from the beam axis, respectively, in a $B = 4$ T magnetic field. 100 000 complete pixel and strip hits were generated, down to the level of individual channels. For simplicity, the charge drift direction was assumed to be parallel with the electric field, perpendicular to the silicon unit. Hence the change in direction due to the $\mathbf{E} \times \mathbf{B}$ effect was omitted.

The addition of local particle direction and energy loss information will make the residuals of the hit position measurement smaller. In case of pixels the deviations from the true value can be decomposed into projections parallel and perpendicular to the passage of the particle (Fig. 12). In both cases the proposed model (labeled as Fitter) gives better results than the weighted or first-last methods introduced in Sec. 3.1. The differences are mostly seen in the perpendicular direction. The measured Gaussian resolutions as a function of the number of pixels in the cluster for all three discussed methods are shown in Fig. 13, in some cases reaching $1 \mu\text{m}$ levels. The corresponding plots of residuals and position resolution for strips are shown in Fig. 14, again the fitter giving the best results.

The resolution of the position estimate can be calculated hit by hit using the observed Fisher information (Sec. 2.4). Residuals of the reconstructed hit position for pixels and strips are shown in Fig. 15. The measured values from comparison of reconstructed and simulated positions are plotted together with the distribution *predicted* from the errors of the fitted parameters. There is a very good agreement between observed and predicted values. Note that for pixels the cross-correlation term can also be deduced giving valuable input for track refit.

4. Estimation of hit energy deposit

The deposited energy Q in the cluster could be plainly estimated with the sum of the individual channel deposits y_i :

$$Q_{\text{Sum}} = \sum_i y_i$$

but this approach clearly has various biases (Sec. 2.2).

The deposited energy can be lost during clustering, because the deposit can be below the channel threshold (left truncation). The average lost deposit $\langle y \rangle$ can be estimated using the discussed microscopical model. Example values as function of path length l for several threshold settings ($t = 6, 8$ and 10 keV) are shown in Fig. 16-left, for particles with $\beta\gamma = 3.16$. In case of large l the average lost deposit is close to the threshold, $\langle y \rangle \approx t$, because the probability density function $p(y|l)$ is very steep for low y values. If the path length l is small the average lost deposit will be simply

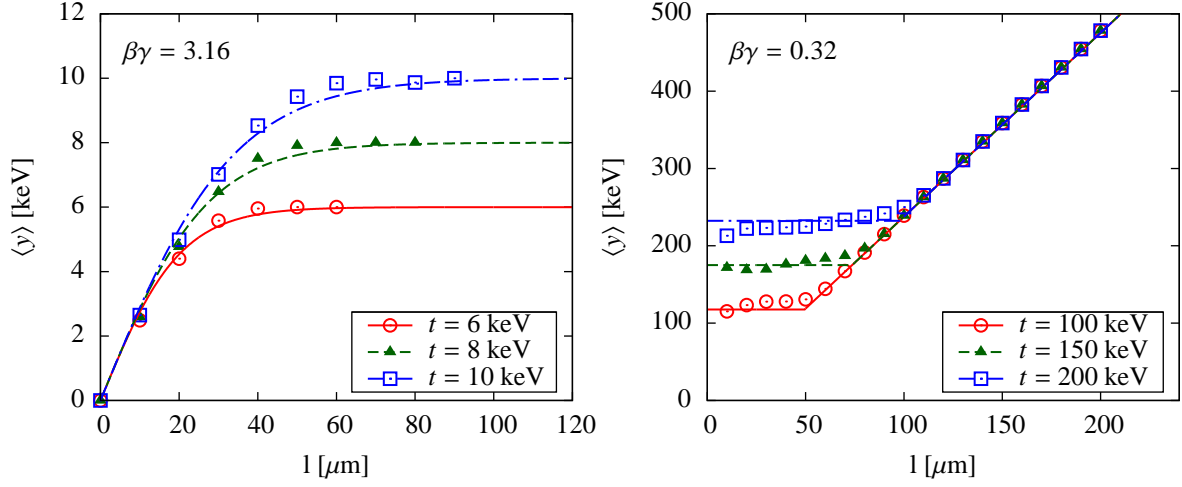


Figure 16: The average lost deposit $\langle y \rangle$ as function of the path length l for several threshold. Left: deposits below threshold with $t = 6, 8$ and 10 keV, for particles with $\beta\gamma = 3.16$. Right: deposits above censoring level with $t = 100, 150$ and 200 keV, for particles with $\beta\gamma = 0.32$. The curves show the functional forms of Eq. (18) and Eq. (19), respectively.

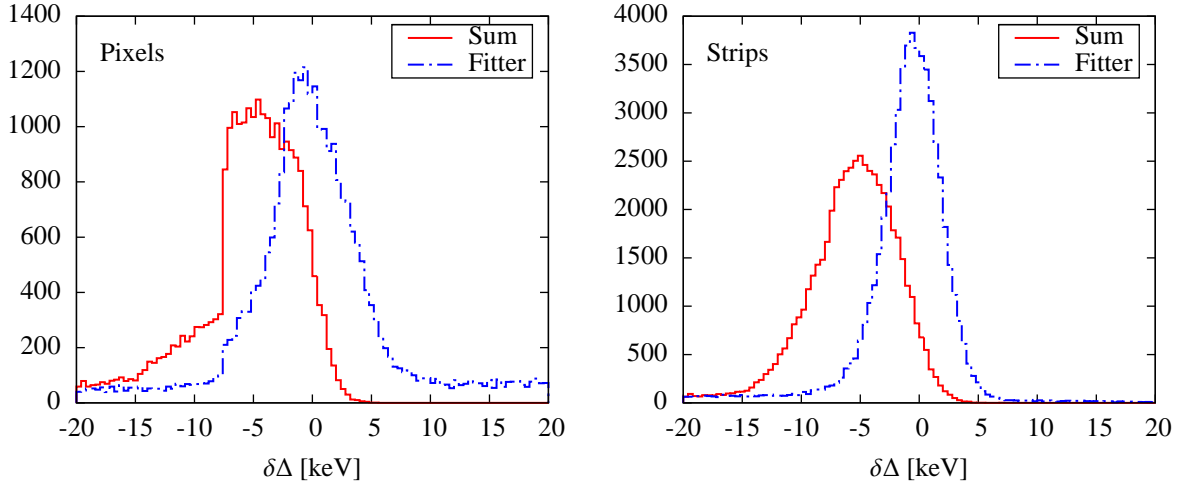


Figure 17: Residuals of the reconstructed deposited energy of the hit cluster for pixels (left) and strips (right). The result of the simple sum and the proposed fitter are compared.

$\langle y \rangle \approx \varepsilon l$. These observations can be successfully described and matched with simulated data (Fig. 16-left) using the following formula:

$$\langle y \rangle_{y < t} \approx t \tanh\left(\frac{\varepsilon l}{t}\right). \quad (18)$$

The measured value can also be saturated, when the deposit is above censoring level (right censoring). Example values as function of path length l for several threshold settings ($t = 100, 150$ and 200 keV) are shown in Fig. 16-right, for particles with $\beta\gamma = 0.32$. In case of small l the average lost deposit can be estimated as

$$\langle y \rangle \approx \frac{\int_t y \exp[-\nu y / \sigma_\Delta(t)]}{\int_t \exp[-\nu y / \sigma_\Delta(t)]} = t + \frac{\sigma_\Delta(t)}{\nu}.$$

If the path length l is large the average lost deposit will be simply $\langle y \rangle \approx \varepsilon l$. These observations can be successfully described and matched with simulated data (Fig. 16-right) using the following formula:

$$\langle y \rangle_{y>t} \approx \max\left(t + \frac{\sigma_{\Delta}(t)}{v}, \varepsilon l\right). \quad (19)$$

4.1. Coupled signals

In case of strips the observed signals are correlated due to the capacitive coupling of the neighboring strips and cross-talk. This effect can be modelled by a tridiagonal matrix:

$$C = \begin{pmatrix} 1 - 2\alpha & \alpha & & 0 \\ \alpha & 1 - 2\alpha & \ddots & \\ & \ddots & \ddots & \alpha \\ 0 & & \alpha & 1 - 2\alpha \end{pmatrix}$$

where $\alpha > 0$, such that the measured deposits y' can be obtained from the original ones y by

$$y' = Cy.$$

Since the signals are coupled, $\sum_i \chi_i^2$ would sum dependent values making the minimization false. The coupling should be first undone by applying C^{-1} to the measured deposits. The inverse of C can be exactly calculated [12], furthermore if $\alpha \ll 1$ it is well approximated by

$$C^{-1}_{ij} = -\frac{(2 - 1/\alpha)^{|i-j|-1}}{\alpha}.$$

Note that due to the presence of signals below threshold and saturated values the decoupling is not exact. The measured deposit in the i th channel is either given, or subject to inequalities:

$$(Cy)_i = y'_i \quad \text{or} \quad (Cy)_i < t \quad \text{or} \quad (Cy)_i > t.$$

In that sense a system of equalities and inequalities has to be solved for y . The problem can be easily handled with the tools of linear programming [11, 13], the OOQP package [14], available in ROOT [15] under MATH/QUADP, could be used for this purpose. The solution is not unique, hence the minimization of a scalar product $\mathbf{c}y'$ is also required. In this case it is advantageous to set $\mathbf{c} = (1, \dots, 1)$. This way those solution will be selected where $\sum_i y_i \equiv Q_{\text{Fitter}}$ is minimal.

In fact the situation is even more complicated due to the presence of detector and readout noise. Assuming a Gaussian noise with standard deviation σ , the χ^2 contribution of the i th channel is

$$\begin{aligned} \chi_{y'}^2 &= \left(\frac{y'_i - (Cy)_i}{\sigma}\right)^2 \\ \chi_{y'<t}^2 &\approx \begin{cases} \frac{1}{2} \left(\frac{t-(Cy)_i}{\sigma} - 2\right)^2, & \text{if } \frac{t-(Cy)_i}{\sigma} - 2 < 0 \\ 0, & \text{otherwise} \end{cases} \\ \chi_{y'>t}^2 &\approx \begin{cases} \frac{1}{2} \left(\frac{t-(Cy)_i}{\sigma} + 2\right)^2, & \text{if } \frac{t-(Cy)_i}{\sigma} + 2 > 0 \\ 0, & \text{otherwise.} \end{cases} \end{aligned}$$

Here, in case of the inequalities, the exact values

$$P(y < t|m) = \frac{1}{2} \left[1 + \operatorname{erf}\left(\frac{t-m}{\sigma\sqrt{2}}\right) \right]$$

were approximated as

$$\chi^2 = -2 \log P \approx \begin{cases} \frac{1}{2} \left(\frac{t-m}{\sigma} - 2 \right)^2, & \text{if } \frac{t-m}{\sigma} - 2 < 0 \\ 0, & \text{otherwise.} \end{cases}$$

In order to keep the minimization away from unphysical negative y_i values, a penalty $(Cy)_i/\sigma)^2$ is added if $(Cy)_i < 0$.

The joint chi-square $\sum \chi_{y_i}^2$ is a positive definite quadratic function of the original deposits y_i . The first and second derivatives with respect to y_i components are easily calculable and the function can be minimized with Newton's method, in few iterative steps.

If some y_i values are negative at the minimum, the one with lowest value is fixed to 0, the minimization is redone. In the end we have a minimum joint chi-square with all the y_i values being non-negative. At the minimum the total charge and its variance are given as

$$Q = \sum_i y_i, \quad \sigma_Q^2 = \sum_{i,j} \text{Var}(y_i, y_j),$$

respectively.

4.2. Results

The details of the simulation are the same as they were described in Sec. 3.6. Residuals of the reconstructed deposited energy of the hit cluster are shown in Fig. 17, for pixels and strips. The result of the simple sum and the proposed fitter are compared. The sum has a -5 keV shift for both configurations which is a 5% effect for minimum ionizing particles along a $300 \mu\text{m}$ path in silicon. At the same time the fitter has practically no bias and a better resolution.

5. Estimation of the most probable differential energy loss for tracks

Having the proper hit energy deposits y_i , the next step is to estimate the most probable differential energy loss for the whole trajectory. The task is very similar (Eq. (16)), but only ε has to be optimized, because the path lengths l_i are given from track finding,

$$\chi^2(\varepsilon) = \sum_i \chi_{y_i}^2(\Delta(\varepsilon, l_i)).$$

Since the terms on the right contain linear or positive definite quadratic functions (Eqs. (11)-(13)) a fast convergence with Newton's method is guaranteed.

The derivatives are

$$\begin{aligned} \frac{\partial \chi_y^2(\Delta)}{\partial \Delta} &= \begin{cases} \frac{-2y}{\sigma_\Delta(y)}, & \text{if } \Delta < y - \nu\sigma_\Delta(y) \\ \frac{2(\Delta-y)}{\sigma_\Delta(y)^2}, & \text{if } \Delta \geq y - \nu\sigma_\Delta(y) \end{cases} \\ \frac{\partial \chi_{y < t}^2(\Delta)}{\partial \Delta} &= \begin{cases} 0, & \text{if } \Delta < t - \sigma_\Delta(t) \\ \frac{2(\Delta-t+\sigma_\Delta(t))}{\sigma_\Delta(t)^2}, & \text{if } \Delta \geq t - \sigma_\Delta(t) \end{cases} \\ \frac{\partial \chi_{y > t}^2(\Delta)}{\partial \Delta} &= \begin{cases} -\frac{1}{\sigma_\Delta(t)}, & \text{if } \Delta < t + \sigma_\Delta(t) \\ 0, & \text{if } \Delta \geq t + \sigma_\Delta(t). \end{cases} \end{aligned}$$

Only the following second derivatives are non-zero:

$$\begin{aligned} \frac{\partial^2 \chi_y^2(\Delta)}{\partial \Delta^2} &= \frac{2}{\sigma_\Delta(y)^2}, & \text{if } \Delta \geq y - \nu\sigma_\Delta(y) \\ \frac{\partial^2 \chi_{y < t}^2(\Delta)}{\partial \Delta^2} &= \frac{2}{\sigma_\Delta(t)^2}, & \text{if } \Delta \geq t - \sigma_\Delta(t). \end{aligned}$$

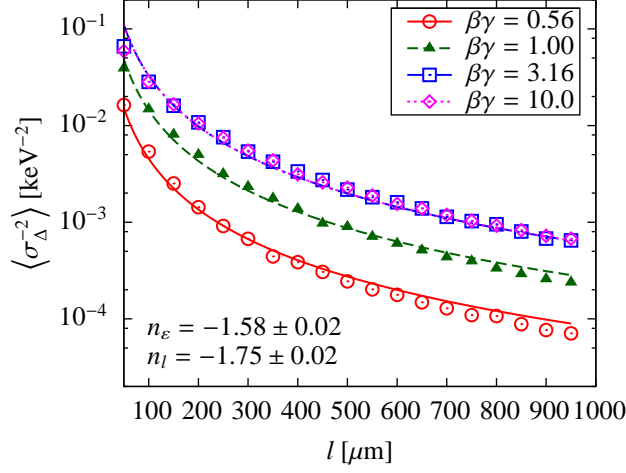


Figure 18: The expectation value of σ_{Δ}^{-2} as function of path length l at several $\beta\gamma$ values (points). The curves show the functional form defined in Eq. (20). The corresponding fitted powers for ε and l are also indicated.

5.1. Resolution

The dependence of the standard deviation of the ε estimate can be obtained as (Sec. 2.4):

$$I(\varepsilon) = \frac{1}{2} \sum_i E \left[\frac{\partial^2 \chi_i^2}{\partial \varepsilon^2} \right]$$

where the second derivative is

$$\frac{1}{2} \frac{\partial^2 \chi_i^2}{\partial \varepsilon^2} = \begin{cases} \left(\frac{l_i [1 + a \log(l_i/l_0)]}{\sigma_{\Delta}(y)} \right)^2, & \text{if in the Gaussian part} \\ 0, & \text{if in the exponential part.} \end{cases}$$

According to the fit shown in Fig. 18 the expectation value of σ_{Δ}^{-2} is a power function of ε and l :

$$\langle \sigma_{\Delta}^{-2} \rangle \propto \varepsilon^{-1.6} l^{-1.8}. \quad (20)$$

With that, also approximating the factor $a \log(l_i/l_0)$ in the range $l = 50 - 1000 \mu\text{m}$,

$$\sigma^2(\varepsilon) \propto \frac{\varepsilon^{1.6}}{\sum_i l_i^{0.2}}.$$

It is clear that the relative resolution $\sigma(\varepsilon)/\varepsilon$ only slightly depends on ε , hence $\log \varepsilon$ is a convenient and uniform estimator. Since the exponent of the path length is also small (0.2), it is not the total thickness of the silicon, but the *number of independent measurements* that matters. For a given total path length the relative resolution is proportional to $n^{-0.4}$, where n is the number of independent measurements. The reason for that originates in the non-Gaussian nature of the energy deposit distribution. Grouped measurements would have worse resolution unlike in the Gaussian case where the resolution would stay unchanged.

5.2. False hit removal

Since the association of hits to trajectories is not always unambiguous some hits do not belong to the proper track. Although their measured deposit is correct, the calculated path length can be false. Assuming that there is at most one false hit in a trajectory it can be detected and removed: the exclusion of the outlier hit decreases the joint chi-square of the trajectory by a considerable amount.

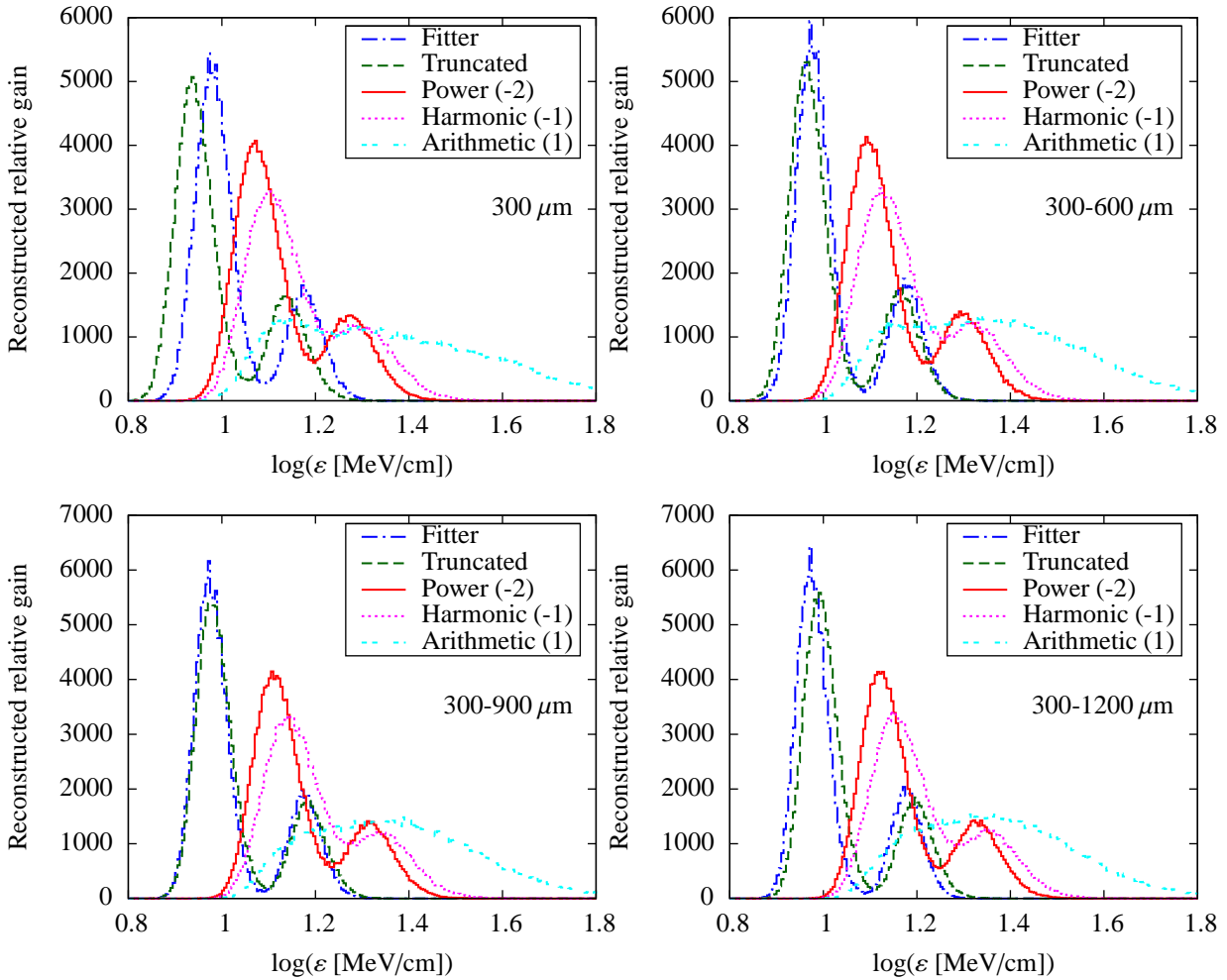


Figure 19: Distribution of the estimated most probable differential energy loss values at reference length (ε), obtained with the four detector layer settings. Several methods are shown: this maximum likelihood fitter, truncated mean, power mean (power -2), harmonic mean (-1) and arithmetic mean (1).

5.3. Distribution of the estimator

Although the most probable value of ε is estimated, it is equally important to deduce, or also estimate, its distribution. Although the variance of the estimate is given, the original probability density is a skewed function: the estimator is not expected to follow a perfect Gaussian distribution. The distribution of the joint χ^2 could be determined track by track with detailed Monte Carlo simulation, but this possibility would have huge computational demands and timing issues.

Are there other methods that could be used to estimate the distribution of the estimator? One of them is the *statistical bootstrap* [16], that is a random sampling with replacement from the original dataset. The so called *jackknife* method [16] can also be considered where the estimate is systematically recomputed leaving out one observation at a time from the sample. Both methods can be used to estimate bias, variance and the shape of the distributions. It can be shown that the jackknife method cancels biases with terms proportional to $1/n$ and $1/n^2$. A problem common to both resampling methods is that they do not work if the sample size is small. Since here we deal sometimes with tracks with as few as two or three measurements these approaches are not viable. For example, in case of the jackknife method, the variance of the subsamples will have large errors if the subsample consist of only one or two measurements.

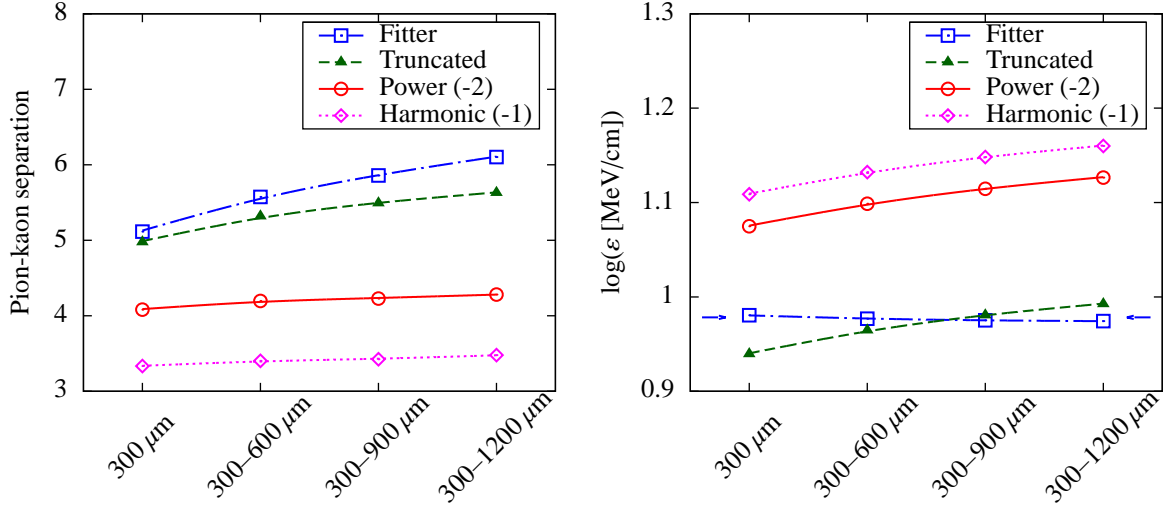


Figure 20: Left: pion-kaon separation power for four detector layer settings, using several methods: this maximum likelihood fitter, truncated mean, power mean (power -2), and harmonic mean (-1). Right: most probable differential energy loss values at reference length ($\log \varepsilon$), shown for the four detector layer settings. The horizontal arrows show the expected theoretical value. Lines are drawn to guide the eye.

As a solution, the shape of the $\log \varepsilon$ distribution could be determined by energy deposit *regeneration*. A measured track is used to construct the shape distribution of a given particle species (mass m), if its measured ε value is compatible with the corresponding value at a given p/m . While all kinematical parameters and path lengths of hits in silicon are kept, all energy deposit values are randomly regenerated using assumed p/m values, as described in Sec. 2.5. The chosen procedure ensures meaningful shape determination even for tracks with very few hits and exploits the success of the energy loss model seen at the hit level.

5.4. Results

In order to demonstrate track level applications a very simple detector model was used: 16 layers of silicon at normal incidence. The orientation of layers and the bending of particle trajectories are taken into account by defining four different layer settings:

- all layers are 300 μm thick (labeled as 300 μm);
- four groups of layers, each containing four 300, 400, 500 and 600 μm thick layers (300-600 μm);
- four groups of layers, each containing four 300, 500, 700 and 900 μm thick layers (300-900 μm);
- four groups of layers, each containing four 300, 600, 900 and 1200 μm thick layers (300-1200 μm).

For the study the 100 000 pions and 30 000 kaons were generated at total momentum $p = 0.8 \text{ GeV}/c$, and a Gaussian noise with 1 keV standard deviation was added to each energy deposit.

Distribution of the estimated most probable differential energy loss values at reference length ($\log \varepsilon$), obtained with the four detector layer settings, are shown in Fig. 19 (Fitter). Results of several other methods working with the differential energy deposit values y_i/l_i are also plotted: truncated mean (average of the lowest half of the y_i/l_i numbers, 0-50% truncation) [17, 18]; as well as those using all measurements, such as power mean (power -2), harmonic mean (power -1) and arithmetic mean (power 1). While the maximum likelihood fitter gives the best results in all the cases, power means have much worse resolution. The truncated mean performs surprisingly well.

The resulted distributions can be fitted with sum of Gaussians. The performance can be further examined by plotting the pion-kaon separation power, defined as $|m_1 - m_2|/[(\sigma_1^2 + \sigma_2^2)/2]^{1/2}$, where m_i and σ_i are the means and standard deviations for pions and kaons, respectively. Comparisons including estimators listed above are shown in

Fig. 20-left, for the four detector layers settings. Again the maximum likelihood fitter gives the best result over the others. The separation power increases if longer hit path lengths or thicker detectors are used (compare with observations in Sec. 5.1).

Ideally the mean of the $\log \varepsilon$ estimates should not depend on path lengths and detector details. The dependence of the mean for the four layers settings is given in Fig. 20-right. The horizontal arrows show the expected theoretical value. It is clear that the maximum likelihood fitter provides stable means, while the others show a pronounced increase. Although for these latter the dependencies could be compensated, in case of tracks with varying path length distribution only the proposed method would perform appropriately.

6. Detector gain calibration with tracks

In order to determine the multiplicative gain correction g for a chip, terms such as

$$X_j^2(g) \equiv \chi_{gy_j}^2(\Delta)$$

should be summed for collected hits and the sum minimized by varying g . The partial derivatives of χ_y^2 are

$$\begin{aligned} \frac{\partial \chi_y^2(\Delta)}{\partial y} &= \frac{2b}{\sigma_\Delta(y)} + \begin{cases} \frac{2\nu\sigma_\Delta(\Delta)}{\sigma_\Delta(y)^2}, & \text{if } \Delta < y - \nu\sigma_\Delta(y) \\ -\frac{2(\Delta-y)\sigma_\Delta(\Delta)}{\sigma_\Delta(y)^3}, & \text{if } \Delta \geq y - \nu\sigma_\Delta(y) \end{cases} \\ \frac{\partial^2 \chi_y^2(\Delta)}{\partial y^2} &= -\frac{2b^2}{\sigma_\Delta(y)^2} + \\ &+ \begin{cases} -\frac{4\nu b\sigma_\Delta(\Delta)}{\sigma_\Delta(y)^3}, & \text{if } \Delta < y - \nu\sigma_\Delta(y) \\ \frac{2[\sigma_\Delta(y)+3b(\Delta-y)]\sigma_\Delta(\Delta)}{\sigma_\Delta(y)^4}, & \text{if } \Delta \geq y - \nu\sigma_\Delta(y). \end{cases} \end{aligned}$$

With that

$$\begin{aligned} \frac{\partial X_j^2}{\partial g} &= \left(\frac{y}{g} \frac{\partial \chi^2}{\partial y} \right) \Big|_{y=gy_j} \\ \frac{\partial^2 X_j^2}{\partial g^2} &= \left(\frac{y^2}{g^2} \frac{\partial^2 \chi^2}{\partial y^2} \right) \Big|_{y=gy_j} \end{aligned}$$

where $y = gy_j$ should be substituted.

6.1. Complete gain calibration

The cross-calibration can be performed in the following steps.

1. With help of a preliminary gain calibration estimate ε for each track. Select pion-like tracks and collect the values of $\beta\gamma$, path length and deposit of each hit, and store them for every chip separately. For each chip minimize the joint chi-square of all selected hits by varying the gains. The minimization is best performed by a golden section search [19] first, in order to get near the region of the minimum, followed by a refinement using Newton's method.
2. Using the updated gains select only those tracks which are certainly pions, kaons, protons or decay daughters of abundantly produced hadrons ($K_S^0 \rightarrow \pi^+\pi^-$, $\Lambda \rightarrow p\pi^-$, $\bar{\Lambda} \rightarrow \bar{p}\pi^+$), or conversion products ($\gamma \rightarrow e^+e^-$). Collect their hits for every chip separately and minimize again the joint chi-square chip by chip by varying the gains with similar methods as above.
3. Finally, using all tracks, minimize their joint chi-square simultaneously. This can be accomplished by nested minimizations. For a given set of gains the ε_i values are determined for each track separately in the course of a local minimization. The gains of chips can be highly correlated since tracks often traverse detector units which are behind each other or very close in space (double-sided units), but also due to manufacturing details. In case of 10^4 - 10^5 chips the covariance matrix needed for the minimization step is sparse, but huge. It is usually numerically difficult to invert. In order to have a treatable problem the detector units with highest correlation are identified, this way forming a covariance matrix with a block diagonal structure. This latter is already easily inverted and the Newtonian step can be computed.

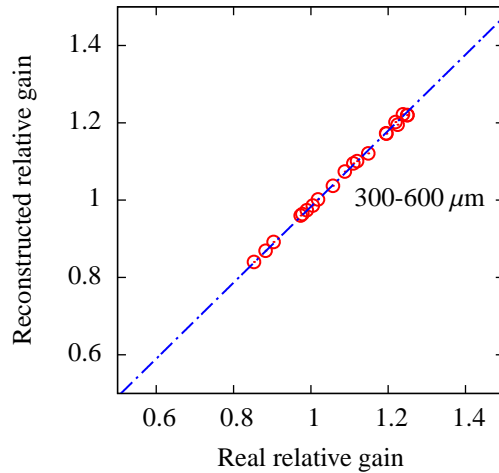


Figure 21: Reconstructed relative gains as function of the real values, shown for the 16 layers used in the detector simulation.

6.2. Results

The details of the simulation are the same as they were described in Sec. 5.4, but now the initial gains of the layers were set randomly in the range 0.8–1.2. Only the first step in the list of Sec. 6.1 was performed. The extracted relative gains as function of the real values are shown in Fig. 21, for all the 16 layers used. While the gains are steadily smaller by about 1% (bias), they have an excellent relative precision.

7. Conclusions

In this work a new analytical energy loss model for charged particles in silicon was introduced. It has few parameters and it is based on the recognition of a special connection between the distribution of the deposited energy and the most probable energy loss. Its use was demonstrated through several examples. With help of measured charge deposits in pixels or strips of hit clusters their position and energy can be estimated with better accuracy and much less bias. Deposits below threshold and saturated values are treated properly, resulting in a wider dynamic range. The model was successfully applied to track differential energy loss estimation and to detector gain calibration tasks, again showing a performance superior to standard methods.

Acknowledgements

The author wishes to thank to Sándor Hegyi, András László and Dániel Barna for helpful discussions. This work was supported by the Hungarian Scientific Research Fund with the National Office for Research and Technology (K 81614, H07-B 74296), and the Swiss National Science Foundation (128079).

References

- [1] O. Ullaland, Update in particle identification, Nucl. Phys. Proc. Suppl. 125 (2003) 90–99. doi:10.1016/S0920-5632(03)90972-8.
- [2] H. Yamamoto, dE/dx particle identification for collider detectors arXiv:hep-ex/9912024.
- [3] H. Bichsel, Straggling in thin silicon detectors, Rev. Mod. Phys. 60 (1988) 663–699. doi:10.1103/RevModPhys.60.663.
- [4] K. Nakamura, et al., Review of particle physics, J.Phys.G G37 (2010) 075021. doi:10.1088/0954-3899/37/7A/075021.
- [5] H. Bichsel, Inelastic electronic collision cross sections for Monte Carlo calculations, Nucl. Instrum. Meth. B52 (1990) 136. doi:10.1016/0168-583X(90)2990581-E.
- [6] H. Bichsel, A method to improve tracking and particle identification in TPCs and silicon detectors, Nucl. Instrum. Meth. A562 (2006) 154–197. doi:10.1016/j.nima.2006.03.009.

- [7] M. Brigida, et al., A new Monte Carlo code for full simulation of silicon strip detectors, *Nucl. Instrum. Meth.* A533 (2004) 322–343. doi:10.1016/j.nima.2004.05.127.
- [8] B. Efron, D. V. Hinkley, Assessing the accuracy of the maximum likelihood estimator: Observed versus expected Fisher Information, *Biometrika* 65 (1978) 454–487. doi:10.1093/biomet/65.3.457.
- [9] Y. Allkofer, et al., Design and performance of the silicon sensors for the CMS barrel pixel detector, *Nucl. Instrum. Meth.* A584 (2008) 25–41. doi:10.1016/j.nima.2007.08.151.
- [10] M. Swartz, D. Fehling, G. Giurgiu, P. Maksimovic, V. Chiochia, A new technique for the reconstruction, validation, and simulation of hits in the CMS pixel detector, *PoS VERTEX2007* (2007) 035.
- [11] W. H. Press, B. P. Flannery, S. A. Teukolsky, W. T. Vetterling, *Numerical Recipes: The Art of Scientific Computing*; 3rd ed., Cambridge Univ. Press, Cambridge, 2007.
- [12] J. W. Lewis, Inversion of tridiagonal matrices, *Numer. Math.* 38 (1982) 333–345. doi:10.1007/BF01396436.
- [13] E. D. Nering, A. W. Tucker, *Linear programs and related problems*, Academic Press Professional, Inc., San Diego, CA, USA, 1993.
- [14] E. M. Gertz, S. J. Wright, Object-oriented software for quadratic programming, *ACM Trans. Math. Softw.* 29 (1) (2003) 58–81. doi:10.1145/641876.641880.
- [15] R. Brun, F. Rademakers, ROOT: An object oriented data analysis framework, *Nucl. Instrum. Meth.* A389 (1997) 81–86. doi:10.1016/S0168-9002(97)00048-X.
- [16] J. Shao, D. Tu, *The jackknife and bootstrap*, Springer series in statistics, Springer Verlag, 1995.
- [17] R. C. Fernow, *Introduction to experimental particle physics*, Cambridge University Press, 1986, pages 253-255.
- [18] C. Grupen, B. Shwartz, H. Spieler, *Particle Detectors*, 2nd Edition, Cambridge University Press, 2008, pages 278-280.
- [19] J. Kiefer, Sequential minimax search for a maximum, *Proc. Amer. Math. Soc.* 4 (1953) 502–506. doi:10.2307/2032161.